J. Fluid Mech. (1999), *vol.* 389, *pp.* 137–168. Printed in the United Kingdom

Dynamics of two interacting bubbles in an acoustic field

By TIBERIU BARBAT, NASSER ASHGRIZ AND CHING-SHI LIU

Department of Mechanical and Aerospace Engineering,
State University of New York at Buffalo, Buffalo, NY 14260, USA
e-mail:ashgriz@eng.buffalo.edu

(Received 23 May 1997 and in revised form 21 December 1998)

This paper contains theoretical and experimental results on the relative motion of two pulsating spherical bubbles along their line of centres, in a liquid subjected to an acoustic field. The motion is caused only by the secondary Bjerknes forces. The linear theory for the secondary Bjerknes forces is modified by introducing a model for the coupling between the pulsations of the interfaces. The secondary effects introduced by this model are determined by the frequency indices of the bubbles, defined as the ratio of the forcing frequency to the resonance frequency of each bubble. The equations of motion are set up with the conservative Lagrangian formalism. This approach allows an analytical study of all the possible patterns of motion and the identification of the set of governing parameters: total energy and interaction coefficient. A pair of bubbles driven far from their resonance frequencies may attract or repel, depending on whether their frequency indices are respectively on the same side or on either side of unity. For forcing frequencies close to resonance, the proposed model predicts a new pattern of relative motion, namely a periodic motion (oscillations) around an equilibrium bubble separation. The experimental study identifies this new periodic pattern of motion, for acoustically levitated bubbles of nearly equal sizes, forced near their resonance frequency. A quantitative study on the variation of the relative velocity with the separation between the bubbles shows that the conservative model for the motion holds for large and moderate separations. The following information is reported: (*a*) a classification of the pairs of bubbles, based upon their phase difference in oscillations; (*b*) a model for the coupling of the pulsations of two bubbles; (*c*) formulas for the interaction force field of two pulsating bubbles, for all of the categories; (*d*) a study of all possible patterns of relative motion (collisions, scattering and oscillations), with their conditions of occurrence; (*e*) experimental data for two attracting bubbles; (*f*) experimental data for two oscillating bubbles.

1. Introduction

The interaction between a single bubble and a sound wave is named the 'primary Bjerknes force' after Bjerknes (1906). If the forcing frequency is less than the resonance frequency of the volume pulsations of the bubble, the primary Bjerknes force is oriented along the gradient of the amplitude of the sound wave, and the bubble travels towards pressure anti-nodes. If the forcing frequency is higher than the resonance frequency of the bubble, the primary Bjerknes force is oriented against the gradient of the amplitude of the sound wave, and the bubble moves towards pressure

nodes. Eller (1968) provides the following mathematical description for the primary Bjerknes force, derived for the standing waves case:

$$F_A = \frac{2\pi^2 {R_0}^3 A^2}{3P_0\lambda(1-\omega^2/{\omega_0}^2)} \sin\frac{4\pi z}{\lambda}, \tag{1}$$

where R_0 is the equilibrium radius of the bubble, A is the amplitude of the standing wave, P_0 is the hydrostatic pressure at the location z of the centre of bubble, ω is the forcing angular frequency, ω_0 is the resonance angular frequency of the bubble for pure radial pulsations and λ is the wavelength of the standing wave.

Bjerknes (1906) discovered that two pulsating bubbles attract or repel each other when they oscillate in or out of phase, respectively. The force causing attraction or repulsion is named the 'secondary Bjerknes force'. The primary and the secondary Bjerknes forces were explained by postulating that every body that is moving in an accelerating fluid is subject to a 'kinetic buoyancy' proportional to the product of the acceleration of the fluid, a, multiplied by the mass, ρV, of the fluid displaced by the body: $F_B \sim \rho V a$. Bjerknes hoped to use this phenomenon to explain the effects of electromagnetism and gravitation; the analogy with these forces was supported by the fact that the secondary Bjerknes force is proportional to the sizes of the bubbles and inversely proportional to the square of the distance between their centres.

Dynamical effects associated with the secondary Bjerknes forces are reported in a study concerning cavitation by Kornfeld & Suvorov (1944). They conducted an experimental study of the dynamics of several bubbles close to an oscillating piston, driven around 7.5 kHz. They describe not only the attraction of interacting bubbles, followed by coalescence, and repulsion of small bubbles by a large one, but also a strange zig-zag motion ('dancing bubbles'). The phenomenon received only a qualitative explanation, based on the instability of the motion dominated by the inertia forces.

Blake (1949) reports qualitative experiments with bubbles which form by cavitation in a liquid subject to a 60 kHz acoustic standing wave. Bubbles form at the pressure anti-nodes and migrate to pressure nodes where they 'seem to coalesce' and form bubbles 'up to a millimetre or so in diameter'. His opinion is that the secondary Bjerknes forces can be observed only at small separations, and their effect is, at most, to cause the coalescence of the bubbles.

In a theoretical review concerning possible technologies for degassing liquids, Kapustina (1970) has derived a mathematical model for the attraction of two interacting bubbles in an acoustic field. Drag forces are neglected if the distance r between the centres of the bubbles is larger than a certain r'. Attraction forces yield in this approximation a decrease of r proportional to $t^{3/2}$. For distances smaller than r', a drag term is included in the equation of motion, and a necessary condition for coalescence is derived. Kapustina has studied the patterns of motion due only to the attractive forces.

Another theoretical treatment of the problem of the secondary Bjerknes interactions is contained in the paper by Zabolotskaya (1984). Here, the Lagrangian formalism is applied to a system of two bubbles. Considering the potential and the kinetic energy for the mass of incompressible liquid surrounding the bubbles, the method yields a system of two coupled nonlinear ODEs. The equations are decoupled when the bubble spacing is large enough compared with their size and they reduce to the well-known Rayleigh–Plesset equation for each bubble. Bubbles are assumed to have only radial oscillations, preserving spherical form in time. A certain form of the induced velocity fields is assumed in order to solve the equations. The results of this approach provide the normal modes of pulsation of the bubbles, which change with the distance between the bubbles. More interestingly, it is found that the Bjerknes forces may change sign

during the motion, from an attractive force to a repulsive one, when the two bubbles are driven at a frequency which is slightly different from their resonance frequencies. The interaction force has a very complicated dependence on the relative distance r, and no attempt has been made to obtain analytic solutions. However, three patterns of interaction are identified: attraction at all distances; repulsion at small r, attraction at large r, with a stable equilibrium point (this equilibrium point 'could possibly account for the coalescence of bubbles into swarms'); and attraction at small r, repulsion at large r, with an unstable equilibrium point. The pattern of interaction is strongly dependent on the driving frequency ω, but not on the pressure amplitude A.

Doinikov (1996) has studied the interaction between a gas bubble and a drop, caused by shape oscillations of both interfaces in an acoustic field. The theory developed by Doinikov allows numerical evaluation of the interaction force using several terms of an infinite series, defined by recurrence formulas. Sample computations show that when the forcing frequency is close to the natural frequency of the bubble or the drop, the force can change its sign with the separation, from attraction to repulsion. However, this study is limited to some numerical examples and does not allow an evaluation of the general dynamic behaviour of the system.

Oguz & Prosperetti (1990) have constructed a model for the interaction of two gas bubbles as an application of a general 'virial theorem' derived from Bernoulli's integral for an inviscid, irrotational, unsteady flow. They have assumed a certain form for the potential of the flow field in the incompressible liquid surrounding the bubbles and have obtained a system of nonlinear coupled ODEs. The ODEs are solved numerically in the small time scale of bubble pulsations, without averaging over one period. This technique becomes computationally exhaustive at high forcing frequencies, and it is only practicable for small time intervals of study. The numerical solutions show only two patterns of motion of the system, at least for the limited time intervals (15–25 periods of the applied pressure wave) for which the solution is constructed: attraction and repulsion. An interesting new effect, unpredicted by the linear theory, is that the pattern of interaction may change when the amplitude of the forcing signal is increased. However, the case of a change in the sign of the forces as the motion of the bubbles proceeds is not revealed by this nonlinear numerical study.

The inviscid theoretical approach to the secondary Bjerknes forces of Pelekasis (1991) and the computational results of Pelekasis & Tsamopoulos (1993*a*, *b*) have produced interesting results in a certain range of frequencies, pressure amplitudes and bubble sizes. The surface of each bubble is allowed to deform from the spherical form. The Laplace equation is used to determine the potential of the flow field in the axisymmetric case. This approach predicts repulsive forces if the forcing frequency is located between the two resonance frequencies for volume oscillations of the two unequal bubbles and attractive forces for any other case, including equal-size bubbles. The results of the simulations show agreement with the linear theory with respect to the influence of the separation distance, volumes of the bubbles, forcing amplitude and frequency upon the average acceleration acquired by the bubbles in relative motion. An important nonlinear result is the fact that when the Bond number, $Bo = \rho \bar{a} R^2/\sigma$, based on the average acceleration, $\bar{a}$, the equilibrium radius, R, and the properties of the liquid (ρ the density and σ the surface tension coefficient), lies above a critical value, spherical-cap shapes (surface deformations) appear at the back side (with respect to the acceleration) of the bubbles. However, these numerical simulations are computationally expensive, and they break down easily as the motion proceeds. The numerical stability requirements impose restrictions on the range of Weber and Bond numbers that could be studied with this technique.

Theoretical predictions for bubble–bubble interaction are directly compared with experimental data in the paper by Crum (1975). He has studied experimentally the interaction between air bubbles levitated in an oscillating water tank which is driven at low frequencies (60 Hz) by a mechanical shaker. The gradient of pressure in the plane of motion of the bubbles is measured and found very close to zero. The amplitude of radial oscillations is reported to be very large in these conditions (0.26 mm for a bubble radius of 0.53 mm). In addition, he has provided a simple model for the secondary Bjerknes forces by averaging over one time period the sound field radiated by one bubble at the location of the other one. The result is the following formula for the secondary Bjerknes force:

$$F_B = -\frac{2\pi\rho\omega^2 R_{01}^2 R_{02}^2}{r^2}(\delta R_1)(\delta R_2)\cos\varphi. \tag{2}$$

In this equation, ρ is the density of the surrounding liquid, ω is the angular forcing frequency, δR_i are the amplitudes of the radial pulsations, and φ is the phase difference between the radial oscillations of the bubbles. The equilibrium radii of the two bubbles are denoted by R_{01} and R_{02}. The magnitude of these interactions is found to be almost one third of the buoyancy force on the bubble for a radius of 1 mm. The dynamics of a system consisting of two equal bubbles is then studied with a simple algebraic model. Inertia forces are neglected and the value of the relative velocity is computed by balancing only the interaction force and the drag on the bubble. Crum's theoretical results compare well with his experimental data at low oscillation frequencies. However, his approach uses an undamped pulsation of the interface. Consequently, the phase shift between the harmonic response of the bubble and the unsteady external pressure field can take only two values: 0 or π. This renders only two patterns for the motion, namely attraction or repulsion.

The present paper modifies Crum's theory by considering the interface damping described with the linear theory for a single oscillating bubble of Prosperetti (1977) and by introducing a model for the coupling between bubble pulsations. The new formulas for the interaction force field derived with these changes are used in a comprehensive analytical approach, verified by new experimental data.

In § 2 we present the equations governing the interactive dynamics of two bubbles. Section 2.1 provides the equation for the volume oscillation of a simple bubble subject to an external forcing. Section 2.2 presents the relations for the pressure waves generated by the radial pulsations of each bubble, followed by § 2.3 which provides the force generated by these pressure waves on the neighbouring bubble. Next, the bubble pairs are classified based on the phase difference between their oscillations (§ 2.4). A new model is presented in § 2.5 for the coupling of the two radial pulsations. Finally, the interaction force, with this coupling effect included, is derived in § 2.6 for different classes of bubble pairs. The dynamics of the two interacting bubbles, moving along their line of centres is presented in § 3. Experiments, which support the theoretical findings, are presented in § 4, followed by a summary of the results and concluding remarks in § 5.

2. Physics of bubble–bubble interaction

2.1. *Harmonic response of a single bubble in an acoustic field*

Consider a single bubble, undergoing volume oscillations, in an unbounded liquid domain. The governing equation for bubble pulsations can be derived from the

equilibrium condition for the normal stresses at the interface. The result is the well-known Rayleigh–Plesset (RPNNP) equation:

$$R\ddot{R} + \tfrac{3}{2}\dot{R}^2 = \frac{1}{\rho}\Delta p, \tag{3}$$

where

$$\Delta p = p_{int}(t) - \frac{2\sigma}{R} - \frac{4\mu\dot{R}}{R} - p_{ext}(t).$$

In these relations, μ is the dynamic viscosity of the liquid, $R(t)$ is the time-varying radius of the bubble, p_{int} and p_{ext} are the internal and the external forcing pressure fields, respectively. Assume that the bubble is exposed to a periodic pressure field, represented by

$$p_{ext}(t) = P_0 + A\cos\omega t, \tag{4}$$

where P_0 is the hydrostatic pressure at the location of the bubble centre and A is the amplitude of the forcing field of frequency $f = \omega/2\pi$. The pressure at the interface can be assumed to be spatially uniform if the wavelength of the forcing wave is much larger than the bubble radius. For small amplitudes, Prosperetti (1977) has used a linearized form of (3) to obtain a harmonic solution for bubble radius variation:

$$R(t) = R_0[1 + \epsilon\cos(\omega t + \varphi)], \tag{5}$$

where the response amplitude, ϵ, and the response phase shift with respect to the external pressure field, φ, are computed with the following relations:

$$\epsilon = \frac{A}{\rho\omega_0^2 R_0^2\ \left((q^2-1)^2 + 4\delta^2 q^2\right)^{1/2}} \tag{6}$$

$$\varphi = \arctan\frac{2\delta q}{q^2 - 1}. \tag{7}$$

Here, the frequency index $q \equiv \omega/\omega_0$, and the dimensionless damping coefficient $\delta \equiv \beta/\omega_0$, are defined using the resonance frequency ω_0 for volume oscillations (Prosperetti 1984*a*):

$$\omega_0 = \left(3k\left(\frac{p_0}{\rho R_0^2} + 2\frac{\sigma}{\rho {R_0}^3}\right) - 2\frac{\sigma}{\rho {R_0}^3}\right)^{1/2}, \tag{8}$$

where c is the speed of sound in the liquid phase. Also, the linearized resultant damping $\beta = \beta_v + \beta_{th} + \beta_{ac}$ contains viscous, thermal and acoustic effects, defined as

$$\beta_v = 2\frac{\mu}{\rho {R_0}^2}, \quad \beta_{th} = 2\frac{\mu_{th}}{\rho {R_0}^2}, \quad \beta_{ac} = \frac{\omega^2 R_0}{2c}. \tag{9}$$

Thermal damping effects, μ_{th}, are determined using a procedure involving the properties of the gas inside the bubble (molecular weight M_g, thermal diffusivity D_g, perfect gas constant R_g, adiabatic coefficient k and density ρ_g), properties of the liquid (density ρ, thermal diffusivity D) and the temperature in the liquid T_∞. The procedure is based on a solution for the continuity, momentum and energy equations for radial flow inside the bubble.

Equation (7) contains the influence of the frequency index upon the phase of the pulsations. The frequency index depends on the bubble size (which modifies the resonance frequency ω_0) and on the applied frequency ω. Figure 1 presents the

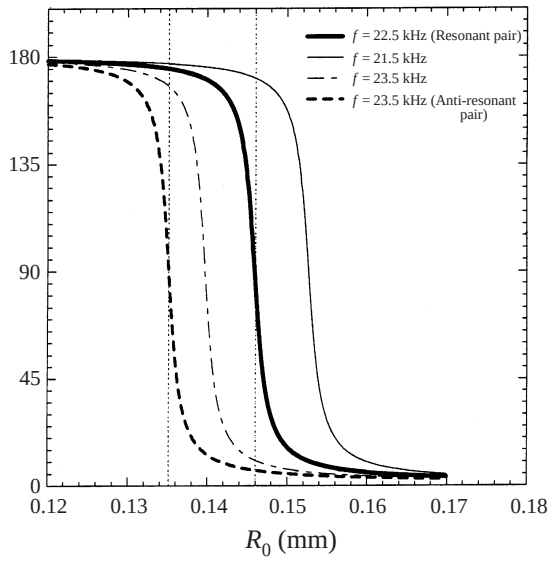

FIGURE 1. Response of a bubble to a sound field: phase shift φ.

variation of the phase shift φ with both of these important physical parameters as described by (7). For a fixed forcing frequency, the phase shift can take any value in the interval $[0, \pi]$, when bubbles of various radii are considered. Bubbles having a frequency index $q \equiv \omega/\omega_0$ less than 1 will oscillate in opposite phase to the external pressure field ($\varphi_i \approx \pi$), while bubbles with q larger than 1 pulsate in phase with the primary wave ($\varphi_i \approx 0$). Even though the transition from $q < 1$ to $q > 1$ is sharp, because of the small value of damping coefficient δ, there is always a range of values for the radius of the bubble which assures $q \approx 1$ and implicitly, $\varphi_i \approx \pi/2$. The graph shows how two nearly equal bubbles (of close radii, 0.1365 and 0.146 mm, represented by vertical dotted lines) can pulsate at phase differences of 0, $\pi/2$ or π, when driven at different frequencies (21.5, 22.5 and 23.5 kHz, respectively). These computations are made considering air bubbles in water at 20 °C, a forcing amplitude $A = 300$ Pa and normal atmospheric pressure above the free surface of the water.

2.2. *Secondary pressure field generated by bubble pulsations*

Consider a single bubble undergoing volume pulsations, while its shape remains spherical. The secondary pressure field induced by its pulsations in the incompressible liquid surrounding the bubble is (Prosperetti 1984*b*)

$$p'(r,t) = \frac{\ddot{V}}{4\pi r} - \tfrac{1}{2}\rho\dot{R}^2\left(\frac{R}{r}\right)^4. \tag{10}$$

The second term can be neglected after performing a scale analysis as described next. Assume that the bubble is driven by a pressure field (4) and its response is a harmonic oscillation of the radius (5). We now compare the amplitudes of the second and the first terms in equation (10):

$$\left|\frac{\rho\dot{R}^2R^4/(2r^4)}{\rho\ddot{V}/(4\pi r)}\right| \approx \frac{\epsilon}{2(r/R)^3}, \tag{11}$$

for small values of the radial response ϵ. Equation (11) shows that for large distances r/R from the bubble, and small forcing amplitudes the second term on the right-hand side of equation (10) is relatively small and can be neglected. Therefore, the oscillating pressure field $p'(r,t)$ generated by bubble pulsations is

$$p'(r,t) \approx \frac{\ddot{V}}{4\pi r} = \frac{R}{r}\left(2\dot{R}^2 + R\ddot{R}\right).$$

A comparison between the amplitudes of the two terms in the $\ddot{V}$ expression reveals that

$$\left|\frac{2\dot{R}^2}{R\ddot{R}}\right| \sim O(\epsilon).$$

Therefore, to the first order in ϵ, the secondary pressure field induced by bubble pulsations is

$$p'(r,t) \approx -\frac{\rho\omega^2 R_0^3 \epsilon}{r}\cos(\omega t + \varphi). \tag{12}$$

The amplitude and phase of the sum of the primary and the secondary pressure fields vary spatially with distance r from the centre of the bubble. When the phase difference φ approaches either of the limits (0 or π), only the amplitude of the pressure distribution is a function of r and the phase shift is spatially uniform.

For bubbles smaller than the resonance size and oscillating out of phase with respect to external forcing, $\varphi \approx \pi$, the amplitude of the pressure field around the bubble is increased. The unsteady part of the pressure field around the bubble is

$$p(r,t) \approx \left(A + \frac{\rho\omega^2 R_0^3 \epsilon}{r}\right)\cos(\omega t). \tag{13}$$

For bubbles larger than the resonance size oscillating in phase with the external forcing, $\varphi \approx 0$, the amplitude of the pressure field is decreased. The unsteady part of the pressure field around the bubble is

$$p(r,t) \approx \left(A - \frac{\rho\omega^2 R_0^3 \epsilon}{r}\right)\cos(\omega t). \tag{14}$$

2.3. *Secondary Bjerknes forces*

Consider now two gas bubbles of nominal radii R_{01} and R_{02}, driven by a pressure field (4), of small amplitude A, into volume pulsations, $R_i(t) = R_{0i}[1 + \epsilon_i \cos(\omega t + \varphi_i)]$, with response amplitudes ϵ_i and phase shifts φ_i. The amplitude of the forcing wave is assumed to be spatially uniform. This assumption is valid when the bubble separation is small compared with the wavelength λ, or when the forcing signal is a plane wave and the bubbles remain in the wavefront plane at any moment of their motion. The linear theory used by Crum (1975) replaces the effect of the secondary pressure field induced by bubble 1 pulsation upon bubble 2 with the time average taken over one period of the surface integral of this pressure field on the surface of bubble 2. The information produced within a period $T = 1/f = 2\pi/\omega$ is lost, but the interaction is reduced to a force-field-type problem, similar to gravitational and electrostatic particle interactions.

Since $\lambda \gg R_{02}$, the integral of p'_1 over the surface S_2 of bubble 2 is approximated as

$$\int\int_{S_2} p'_1(r,t)\,\hat{n}_2\,\mathrm{d}S \approx V_2(t)\,\nabla p'_1, \tag{15}$$

where $\hat{n}_2$ is the outward normal to the interface S_2, and V_2 is the volume enclosed by S_2. For any type of volume pulsation, the force acting on bubble 2 is

$$\mathscr{F}_{12} = -\langle V_2(t)\nabla p'_1(r,t)\rangle, \tag{16}$$

where $\langle\,\rangle$ symbolizes averaging over one period of the forcing field (Prosperetti 1984*b*). The distance r is measured between the bubble centres and the sign convention is that negative values of the force signify 'attraction' and positive values represent 'repulsion'.

Let us consider that the two bubbles respond to the external forcing with pure radial harmonic pulsations, described by equation (5). The time-varying volume of bubble 2 is simply

$$V_2(t) = \tfrac{4}{3}\pi R_{02}^3[1 + \epsilon_2\cos(\omega t + \varphi_2)]^3.$$

The assumption $r \gg R_{01}, R_{02}$ allows the secondary pressure field p'_1 induced by bubble 1 pulsation to be written from (12) as

$$p'_1(r,t) = -\frac{\rho\omega^2 R_{01}^3\epsilon_1}{r}\cos(\omega t + \varphi_1).$$

After averaging in time over one period $2\pi/\omega$, the magnitude of the force $\mathscr{F}_{12}$ acting on bubble 2 along the line of centres, is derived from equation (16) as

$$\mathscr{F}_{12}(r) = -\frac{2\pi\rho\omega^2 R_{01}^3 R_{02}^3}{r^2}\epsilon_1\epsilon_2\cos\varphi\,\Psi(\epsilon_1,\epsilon_2,\varphi), \tag{17}$$

where $\varphi \equiv \varphi_2 - \varphi_1$ is the phase difference between the two pulsations, and

$$\Psi(\epsilon_1,\epsilon_2,\varphi) = 1 - \frac{\epsilon_1\epsilon_2}{\cos\varphi} + \tfrac{1}{4}(\epsilon_1^2 + \epsilon_2^2) + 2\epsilon_1\epsilon_2\cos\varphi + O(\epsilon_1^i\epsilon_2^j), \tag{18}$$

with $i + j \geqslant 3$. The force $\mathscr{F}_{21}$, acting on bubble 1, has the same magnitude, but the opposite orientation.

Equation (17) shows the higher-order nature of the bubble–bubble interaction force, since its magnitude is $O(\epsilon_1\epsilon_2)$. Hence, a rigorous application of the linear theory will render zero interaction forces. Previous analytical studies on secondary Bjerknes forces have considered only the first term in function Ψ and have obtained the well-known formula

$$\mathscr{F}_{12}(r) = -\frac{2\pi\rho\omega^2 R_{01}^3 R_{02}^3}{r^2}\epsilon_1\epsilon_2\cos\varphi, \tag{19}$$

which is identical with equation (2), after substituting the dimensional response amplitudes $(\delta R_i) = \epsilon_i R_{0i}$. This approach is justified by the fact that $\cos\varphi$ is $O(1)$ when $\varphi_1, \varphi_2 = 0$ or π, and function $\Psi(\epsilon_1,\epsilon_2,\varphi) \approx 1$.

Analysis of equation (19) shows that a pair of bubbles which are pulsating in phase ($\varphi = 0$) or at a phase difference less than $\pi/2$ will engage in an attraction motion, for all distances r between the centres of mass. Also, a pair of bubbles pulsating in opposite phase ($\varphi = \pi$) or at a phase difference greater than $\pi/2$ will increase distance in a separation motion for all distances r. Two bubbles having phase difference of $\varphi = \pi/2$ are not supposed to interact according to this formula, since $\mathscr{F}_{12} = \mathscr{F}_{21} = 0$.

A pair of bubbles both driven close enough to resonance frequency, one such that $\varphi_1 \approx 0$ or π, and the other such that $\varphi_2 \approx \pi/2$, can have the following consequences: (*a*) higher values for ϵ_i, implied by the near resonance forcing; (*b*) phase difference of $\varphi \approx \pi/2$, hence $\cos\varphi \sim O(\epsilon_1\epsilon_2)$; and (*c*) coupling between the two pulsations, through the modification of the amplitude of the pressure field around bubble 1, as

described in § 2.2. In these conditions, the second term in the function Ψ becomes $O(1)$ and therefore

$$\Psi(\epsilon_1, \epsilon_2, \varphi) \approx 1 - \epsilon_1\epsilon_2/\cos\varphi.$$

The new force field formula obtained with this approximation is

$$\mathscr{F}_{12}(r) = -\frac{2\pi\rho\omega^2 R_{01}^3 R_{02}^3}{r^2}\epsilon_1\epsilon_2(\cos\varphi - \epsilon_1\epsilon_2). \tag{20}$$

Beside this change in the approximation level, the coupling between the two pulsations, through the induced secondary oscillating pressure fields, will be implemented in the force field model. The secondary pressure field modifies the pressure distribution around the two bubbles and the amplitude of the effective forcing on each bubble changes with the separation distance. This change in forcing leads to a change in the phases φ_i and amplitudes ϵ_i of the responses. Hence, the difference $(\cos\varphi - \epsilon_1\epsilon_2)$ varies as the distance r changes in time. Eventually, the motion can start at positive values for this difference, resulting in attraction forces. As the relative distance decreases, the difference becomes negative and the interaction forces become repulsive. This behaviour may repeat itself, resulting in a new pattern of translational oscillations of the pair of bubbles.

2.4. *Classification of binary systems of bubbles*

The above changes in the interaction force description are significant within a certain range of forcing frequencies and bubble sizes. A classification of the bubble pairs is necessary to identify the conditions requiring the use of the new model for the interaction force. For single bubbles, the frequency index q, defined with respect to the resonance frequency for linear volume oscillations ω_0 is used to classify the types of pulsations. A bubble driven below the resonance frequency has $q_i < 1$ and a phase $\varphi_i \approx \pi$ with respect the forcing wave. A bubble driven above the resonance frequency has $q_i > 1$ and the phase $\varphi_i \approx 0$. If the forcing is close to the resonance frequency then $q_i \approx 1$ and $\varphi_i \approx \pi/2$. Equation (17) imposes only the phase difference φ as the criterion for classifying the interaction between two bubbles: $\varphi = 0$ leads to attraction, while $\varphi = \pi$ results in repulsion forces. Our new model, taking a more detailed approach to how this phase difference is formed, proposes the following classification for binary systems of bubbles:

1. *Non-resonant pair* : φ_1 and φ_2 are both far from $\pi/2$ (q_1, q_2 are far from 1). Here, the interaction force is accurately described by equation (19). Attraction and repulsion are the only patterns of motion possible for this category. There is no equilibrium value for the distance r.

2. *Resonant pair* : One phase shift (take φ_1 for example) is close to $\pi/2$ ($q_1 \approx 1$) and the other (φ_2) approaches π ($q_2 < 1$), while R_{01} and R_{02} have close values. In this case, the phase difference is $\varphi \approx \pi/2$ and $\cos\varphi \sim O(\epsilon_1\epsilon_2)$. Hence, use of (20) in computing the interaction force is appropriate. The amplitude of the pressure field around bubble 1 is increasing as the separation distance r decreases, and so is the response amplitude ϵ_1. In certain conditions, the relative motion could start with an attraction ($\Psi > 0$), but as the term $\epsilon_1\epsilon_2$ becomes larger, the sign of Ψ turns negative and the interaction becomes a repulsion. This case makes possible the existence of a stable equilibrium value for r.

3. *Anti-resonant pair* : $\varphi_1 \approx \pi/2$ ($q_1 \approx 1$) and $\varphi_2 \approx 0$ ($q_2 > 1$), while R_{01} and R_{02} have close values. Again, equations (18) and (20) are used to compute the interaction, but in this case the effect of coupling is a decrease of ϵ_1 as the separation distance

becomes smaller. If the relative motion starts with an attraction, due to $\Psi > 0$, the term $\epsilon_1\epsilon_2$ becomes even smaller during the motion, and the attraction pattern is enhanced. If it starts with an repulsion, due to $\Psi < 0$, then $\epsilon_1\epsilon_2$ increases and the separation forces grow. Thus, this case results in the possibility of having an unstable equilibrium value for r.

2.5. *Model for the coupling of the two pulsations*

Based on the previous considerations for each type of interacting binary system of bubbles, the following models are proposed to replace the coupling between the differential equations of the two interfaces (RPNNP equations):

1. Non-resonant bubbles have completely uncoupled pulsations and the quantities ϵ_i and φ_i do not vary as the two bubbles approach or separate. This assumption stands for large and moderate bubble separations (greater than 3 or 4 radii). However, it is acknowledged as a source of disagreement with the experimental observations for the close approach and collision stages of the motion of two interacting bubbles.

2. Resonant pairs of bubbles have the property of increasing the amplitude of the response ϵ_1 of the bubble driven near resonance as the separation distance r decreases. However, the effect of the secondary waves on the response pulsations is limited to changes in the amplitude ϵ_1, and the phases φ_i are assumed constant during the motion. As a result of this assumption, the pressure field acting on the surface of bubble 1 has an effective amplitude indicated by (13): $A_{ef} = A + \rho\omega^2 R_{02}^3 \epsilon_2/r$. Next, equation (6) is used to derive the response amplitude of the pulsation of the bubble near the resonance, as a function of r:

$$\epsilon_1(r) = \epsilon_{1\infty}\left(1 + \frac{k_{21}}{r}\right). \tag{21}$$

In this equation,

$$k_{21} \equiv \frac{\rho\omega^2 R_{02}^3 \epsilon_2}{A} = R_{02}\theta(q_2),$$

is the *coupling coefficient* implied by our simple superposition model, $\epsilon_{1\infty}$ is the response amplitude when no coupling is considered (for an infinite distance between bubbles), and the function $\theta(q_2)$ is defined on the frequency index q_2 as

$$\theta(q_2) \equiv \frac{q_2^2}{\left((q_2^2 - 1)^2 + 4\delta_2^2 q_2^2\right)^{1/2}}.$$

3. Anti-resonant pairs of bubbles have the property of decreasing the amplitude of the response ϵ_1 of the bubble driven near resonance as r decreases. Following a similar reasoning as above, based on (6) and (14), ϵ_1 varies with r as

$$\epsilon_1(r) = \epsilon_{1\infty}\left(1 - \frac{k_{21}}{r}\right). \tag{22}$$

4. For the resonant and anti-resonant pairs, the amplitude of the response of bubble 2 (driven farther from resonance than bubble 1) is assumed constant during the interaction, since the value of the denominator in function $\theta(q_2)$ is larger than the denominator in $\theta(q_1)$ and, thus, the coupling coefficient k_{12} is negligible.

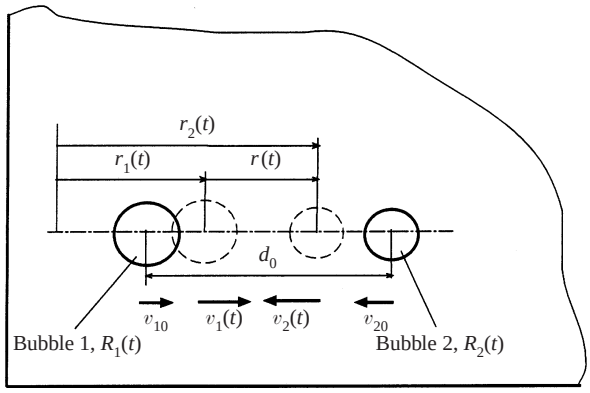

FIGURE 2. Kinematics of a pair of interacting bubbles.

2.6. *Interaction forces for resonant/anti-resonant pairs*

After substituting (21) (respectively, (22)) in (20) and considering terms to r^{-3} only, the magnitudes of the forces are

$$\mathscr{F}_{21}(r) = \mathscr{F}_{12}(r) = -2\pi\rho\omega^2 R_{01}^3 R_{02}^3 \Phi(r), \tag{23}$$

where

$$\Phi(r) \equiv \epsilon_{1\infty}\epsilon_2 \left(\frac{m}{r^2} \mp \frac{k_{21} n}{r^3} \right), \tag{24}$$

where $m \equiv \cos\varphi - \epsilon_{1\infty}\epsilon_2$ and $n \equiv 2\epsilon_{1\infty}\epsilon_2 - \cos\varphi$. In equation (24), the minus sign is for resonant pairs and the plus sign is for anti-resonant pairs. The behaviour of the resonant/anti-resonant pairs of bubbles is governed by the magnitudes of $\cos\varphi$ and $\epsilon_{1\infty}\epsilon_2$: (*a*) if $\cos\varphi < \epsilon_{1\infty}\epsilon_2$, then the interaction force of a resonant pair is repulsive at all distances, while an anti-resonant pair may have an unstable equilibrium value for r; (*b*) if $\epsilon_{1\infty}\epsilon_2 < \cos\varphi < 2\epsilon_{1\infty}\epsilon_2$, then the resonant pair may have a stable equilibrium value for r, while the interaction force of an anti-resonant pair is attractive at all distances; and (*c*) if $\cos\varphi > 2\epsilon_{1\infty}\epsilon_2$, then the resonant pair features attraction forces at all distances and the anti-resonant pair may have a stable equilibrium r. In the following, only case (*b*) will be considered since it is the only one *a fortiori* consistent with the assumption $\cos\varphi \sim O(\epsilon^2)$. Cases (*a*) and (*c*) must include additional assumptions, concerning the lower and the upper limit for $\cos\varphi$, respectively.

For non-resonant pairs, the interaction force can be written in a form similar to (23), but the function Φ is given by

$$\Phi(r) \equiv \frac{\epsilon_1\epsilon_2 \cos\varphi}{r^2}. \tag{25}$$

3. Dynamics of the motion of interacting bubbles

3.1. *Equations of motion*

Consider two given spherical bubbles levitated in a liquid. The levitation condition is provided either by a zero gravity environment, or by balancing the buoyancy with another force (for instance, a primary Bjerknes force). Assume that the bubbles are confined to move only along their line of centres, as depicted in figure 2. There is a forcing pressure field of small amplitude acting on both bubbles, causing only radial

pulsations of the two interfaces. The changes in the pressure distribution around the bubbles are modelled as an interaction force which causes the relative motion of the bubbles.

The drag forces induced by the motion of the bubbles through the surrounding liquid are not considered in the process of writing the equations of motion, such that the system is conservative, and one integral of the motion will be the total energy. The conservative approach to the dynamics of a pair of bubbles allows analytical solutions for the equations of motion to be obtained, which are compared with experimental results in § 4. If drag forces are to be taken into consideration, the theory has to be completed with a drag model, and only numerical solutions are possible for the equations of motion. Crum (1975) used Moore's drag law, which results in a much smaller value for the drag force than the empirical drag coefficient for non-pulsating bubbles. Crum's reasoning for using this model was that '... the impurities on the bubble surface are broken up by the violent pulsations, allowing for interfacial slippage and thus reduced drag ...' . In figure 11, we compare the experimental data for the relative velocity of the two bubbles with the predictions given by the analytical equations derived with the conservative theory. The error due to neglecting the drag is large only for small bubble separations. For small distances between the centres, the force field model for bubble–bubble interaction loses its validity, as well. In one case, we use a numerical solution for the equations of motion including the drag forces (given by Moore's drag law). At the forcing frequencies that are used in the experiments (around 22 kHz), it appears that the drag forces are slightly overestimated by this model. Since the main goal of our paper is to identify all possible patterns of motion, we will restrict the following analysis to the conservative system approach, with no drag forces considered.

The motion of the bubbles is decomposed into a relative motion described by the distance $r(t)$ between the centres and the motion of the centre of mass of the two bubbles. Since $|\mathscr{F}_{12}| = |\mathscr{F}_{21}|$, the motion of the combined centre of mass remains unperturbed by secondary Bjerknes interaction. In order to introduce the effects associated with the acceleration of the liquid surrounding the bubbles, the concept of *virtual mass* (or *induced mass*) is used. For a single bubble the virtual mass is defined as one half of the mass of the volume of liquid displaced. For a pair of bubbles engaged in an accelerated relative motion, the virtual masses must be corrected with terms depending on the instantaneous distance between their centres. However, the correction terms are proportional to r^{-4} and higher-order terms (Basset 1888), while the model which we are proposing in the following is accurate to r^{-3}. The period of the volume pulsations is small compared with the time scale for the translational motion of the interacting bubbles. This allows the assumption that the virtual mass is constant in time and determined by the average radii of the bubbles R_{0i}. Therefore, in the following reasoning, we will consider the virtual mass of the bubble to be constant throughout the motion and given by

$$m_i \equiv \tfrac{2}{3}\pi\rho R_{0i}^3.$$

The dynamic equation for the relative motion may be deduced by applying Newton's second law for each virtual mass localized by r_i ($i = 1, 2$) and combining these two equations in a single ODE for $r = r_2 - r_1$. However, a more convenient approach is that of a two-body Kepler (gravitational) problem, which uses the Lagrange formalism for the particle of *reduced mass*, μ, moving in the interaction force field, at the distance r from the field source (Goldstein 1959). The definition of the reduced mass of the

pair is

$$\mu \equiv \frac{m_1 m_2}{m_1 + m_2},$$

where m_i $(i = 1, 2)$ are the previously defined virtual masses. After substitution, the reduced mass of the pair of bubbles is

$$\mu = \frac{2}{3}\pi\rho R_{01}^3 \frac{\Delta^3}{1 + \Delta^3}, \tag{26}$$

where $\Delta \equiv R_{02}/R_{01}$ is the size ratio. The Lagrangian for this reduced mass is

$$\mathscr{L} = \mathscr{W} - \mathscr{U},$$

where $\mathscr{W} = \mu u^2/2$ is the kinetic energy of the relative motion, u is the relative velocity and $\mathscr{U}$ is the potential generating the interaction force field,

$$\mathscr{F}(r) = -\frac{\partial \mathscr{U}}{\partial r}.$$

The function $\mathscr{U}(r)$ has different forms for non-resonant and resonant/anti-resonant pairs of bubbles. For a non-resonant pair, the potential energy function is proportional to $1/r$ and there is no possibility of a change in the sign of the interaction force, as the relative motion proceeds:

$$\mathscr{U}(r) = -2\pi\rho\omega^2 R_{01}^3 R_{02}^3 \epsilon_1 \epsilon_2 \frac{\cos\varphi}{r}. \tag{27}$$

For a resonant/anti-resonant pair of bubbles, the potential energy function contains a term proportional to $1/r$, generating an attraction/repulsion force, and a term proportional to $1/r^2$, generating a repulsion/attraction component:

$$\mathscr{U}(r) = -2\pi\rho\omega^2 R_{01}^3 R_{02}^3 \epsilon_{1\infty} \epsilon_2 \left[\frac{m}{r} \mp R_{02}\theta(q_2)\frac{n}{2r^2}\right]. \tag{28}$$

The force field generated by the above function may change sign during the motion, from an attraction to a repulsion (or inversely), and an equilibrium value for r results from this fact. The Lagrange equation for the system is

$$\frac{\partial \mathscr{L}}{\partial r} = \frac{\mathrm{d}}{\mathrm{d}t}\left(\frac{\partial \mathscr{L}}{\partial \dot{r}}\right).$$

This leads to the following dynamical equation for the relative motion:

$$\mu\ddot{r} = -\frac{\partial \mathscr{U}}{\partial r}. \tag{29}$$

Equation (29) is non-dimensionalized using R_{01} and $\mathscr{T} \equiv 1/f = 2\pi/\omega$ as the reference length and the reference time interval, respectively. The result is the following non-linear ordinary differential equation of the second order with $x \equiv r/R_{01}$ the unknown function, and $\tilde{t} \equiv t/\mathscr{T}$ the independent variable:

$$\frac{\mathrm{d}^2 x}{\mathrm{d}\tilde{t}^2} = -\frac{\mathscr{K}}{2x^2} + \frac{\mathscr{B}}{x^3}, \tag{30}$$

where $\mathscr{K}$ and $\mathscr{B}$ have different forms for non-resonant and resonant/anti-resonant pairs of bubbles.

For a non-resonant pair, the above coefficients are

$$\mathscr{K} = 24\pi^2(1 + \Delta^3)\,\epsilon_1 \epsilon_2 \cos\varphi, \tag{31}$$

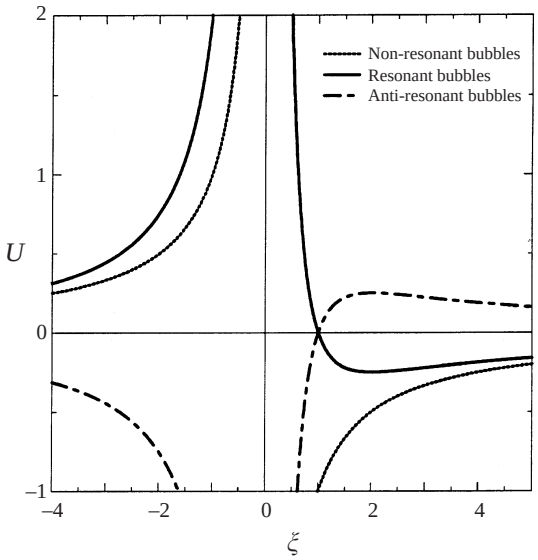

FIGURE 3. The potential function $U(\xi)$, for all classes of interacting bubbles.

and

$$\mathscr{B} = 0. \tag{32}$$

For a resonant pair of bubbles, the coefficients are

$$\mathscr{K} = 24\pi^2(1 + \Delta^3)\, m, \tag{33}$$

and

$$\mathscr{B} = 12\pi^2(1 + \Delta^3)\Delta\theta(q_2)\, n. \tag{34}$$

3.2. *Dynamics of a non-resonant pair of bubbles*

For a non-resonant pair, the dynamical patterns of the pair of bubbles are given by equation (30), with the coefficients (31)–(32). Equation (30) is further modified by scaling the distance with $\mathscr{K}$ and the time with $\mathscr{K}^2$ as

$$\xi \equiv \mathscr{K} x, \tag{35}$$

$$\tau \equiv \mathscr{K}^2 \tilde{t}. \tag{36}$$

The study of the dynamics of the system of two non-resonant bubbles is now reduced to the study of a nonlinear ODE of the following form:

$$\frac{\mathrm{d}^2\xi}{\mathrm{d}\tau^2} = -\frac{1}{2\xi^2}. \tag{37}$$

Equation (37) is used to write the governing dynamical system in a canonic form:

$$\frac{\mathrm{d}w}{\mathrm{d}\tau} = -\frac{1}{2}\frac{1}{\xi^2}, \quad \frac{\mathrm{d}\xi}{\mathrm{d}\tau} = w. \tag{38}$$

A potential energy function $U(\xi) = -1/\xi$ and a total energy $E(\xi, w) = U(\xi) + w^2$ are introduced. The total energy function is constant throughout the motion and its value is established by the initial conditions:

$$E(\xi, w) = \text{constant} = E(\xi_0, w_0), \tag{39}$$

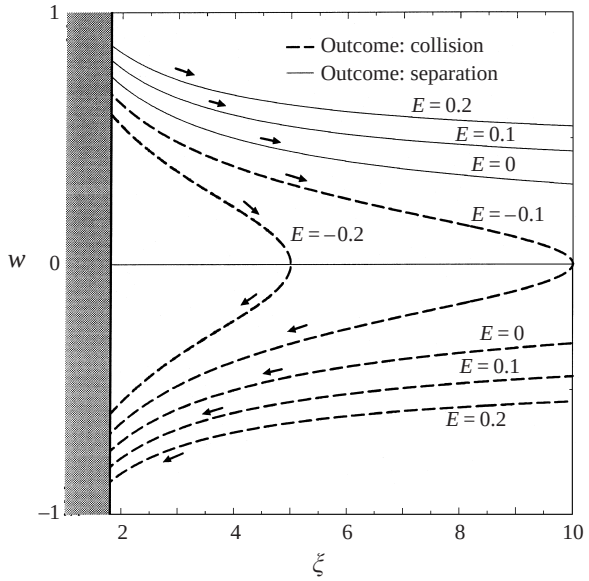

FIGURE 4. Trajectories in the phase plane for the relative motion of a pair of attracting (equal) bubbles.

where $\xi_0 = \mathscr{K} x_0$, $w_0 = v_0/\mathscr{K} = (v_{20} - v_{10})/\mathscr{K}$. Figure 3 shows the variation of the potential energy function $U(\xi)$ in all cases of interaction – the non-resonant pair case is represented with a dotted line. The left branch in the $\xi < 0$ domain corresponds to repulsion forces ($\cos\varphi < 0$), and the right branch to attraction forces ($\cos\varphi > 0$). There are no points of minimum or maximum on these curves, therefore there is no equilibrium state for a pair of non-resonant bubbles.

The physically meaningful values of r, for two spherical bubbles, are $r \geqslant R_{01} + R_{02}$, i.e. the domain defined by $x \geqslant 1 + \Delta$. Hence, there is a limiting value for ξ, corresponding to the collision of the two bubbles:

$$\xi_{lim} = \mathscr{K}(1 + \Delta). \tag{40}$$

3.2.1. *Equal-size bubbles*

Figure 4 represents the trajectories of the system (38)–(39) in the mathematical phase plane (ξ, w) for the particular case of two identical bubbles ($\Delta = 1$). The limiting value for ξ is shown as a thick line. Since $\mathscr{K} > 0$ in this particular case, only values $\xi > \xi_{lim} = 2\mathscr{K}$ having a physical meaning are investigated. The graph in figure 4 is constructed using the following equation for w:

$$w = \pm(E - U)^{1/2} = \pm(E + 1/\xi)^{1/2}. \tag{41}$$

Negative total energy ($E < 0$) leads to collision, regardless of the initial motion of the system, namely an 'approach' ($w < 0$) or a 'separation' ($w > 0$) in the space (ξ, τ). Note that, $w > 0$ implies a real separation motion in the physical space only if the scaling coefficient $\mathscr{K} > 0$ (attractive forces) and, respectively, implies a real approach only if $\mathscr{K} < 0$ (repulsive forces). When the initial motion is such that $w > 0$, the system will continue to increase the distance between the bubbles until a maximum separation $\xi_{max} = -1/E$ is reached and after that the effect of the attraction forces will lead to an approach ending with a collision. Positive total energy ($E \geqslant 0$) leads to separation to infinity (referred to also as 'scattering' of the pair) if initially $w > 0$, and

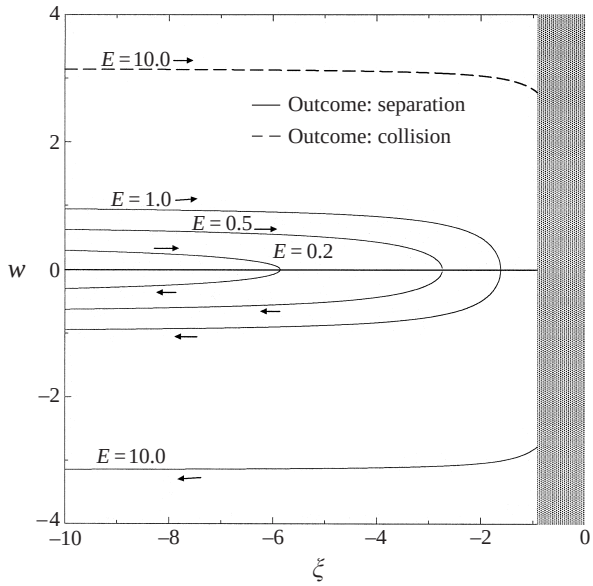

FIGURE 5. Trajectories in the phase plane for the relative motion of two repelling bubbles.

leads to collision if initially $w < 0$. A physical significance for the threshold $E = 0$ can be found by defining an escape relative velocity v_e such that $E = 0$ for any fixed initial distance $x_0 = r_0/R_0$ between the two bubbles. $E = 0$ and $v = v_e$ signify the minimum value for the total energy and, respectively, the minimum positive relative initial velocity which leads to scattering despite attractive secondary Bjerknes forces. Any pair of equal-size bubbles (always attracting) will separate if their initial relative velocity is positive and greater than

$$v_{e1} = 2\sqrt{3}\frac{\epsilon}{x_0^{1/2}}\omega R_0, \tag{42}$$

where $\epsilon = \epsilon_1 = \epsilon_2$ is the response amplitude of the two bubbles of equal radii $R_0 = R_{01} = R_{02}$. A numerical analysis on the values obtained for v_{e1} for bubble sizes between 0.5 mm and 1 mm, forcing frequencies between 1 kHz and 25 kHz and forcing amplitude $A = 300$ Pa, shows that the escape velocity is maximum when the pair of equal bubbles is driven around the resonance ($q \approx 1$). For instance, for bubbles with radii of 0.5 mm, v_{e1} ranges between 0.25 cm s^{-1} (far from resonance, $q = 0.15$) and 78 cm s^{-1} (close to resonance, $q = 1.007$).

3.2.2. *Unequal-size bubbles, repulsive forces*

Assume two bubbles of different sizes, such that bubble 1 is driven above resonance ($q_1 > 1$), and the other is driven below its resonance frequency ($q_2 < 1$). For low amplitudes of the forcing, where nonlinear effects are not important, the two bubbles repel each other and the coefficient $\mathscr{K}$ is negative. Consequently, in the mathematical phase plane (ξ, w), only values $\xi < \xi_{lim} = \mathscr{K}(1 + \Delta)$ have physical meaning. Also, in this case, $w > 0$ represents a real approach motion and $w < 0$ means a real separation between the bubbles.

Figure 5 contains graphs constructed based on equation (41), valid in all cases. Only positive values for the total energy E are acceptable, and there is also a threshold value E_m for the energy. For $0 < E < E_m$, the outcome of the interaction is scattering

of the pair of bubbles, regardless of the sign of the initial relative velocity. For $E > E_m$, the bubbles which have an initial approach relative motion will collide, despite the repulsion due to secondary Bjerknes forces. The threshold value for total energy is found from the limiting condition $E_m = U(\xi_{lim})$. If a phase difference $\varphi \approx \pi$ is assumed between the two pulsations, then $\mathscr{K} = -24\pi^2(1 + \Delta^3)\,\epsilon_1\epsilon_2$ and the result for E_m is

$$E_m = \frac{6}{\theta(q_1)\theta(q_2)}\frac{1}{(1+\Delta)(1+\Delta^3)}. \tag{43}$$

Assuming a given initial distance between the bubbles $x_0 = r_0/R_{01}$, equation (43) can predict the minimum relative velocity v_m required to cause the collision of two repelling bubbles:

$$v_m = -\left(6\epsilon_1\epsilon_2\ \left[\left(1-\frac{1}{x_0}\right) - \Delta + \Delta^2 - \frac{1}{x_0}\Delta^3\right]\right)^{1/2}\omega R_{01}. \tag{44}$$

3.2.3. *Relative velocity*

Equation (41) can be transformed back into the physical quantities, such that an expression for the relative velocity $v = \mathrm{d}r/\mathrm{d}t$ is obtained:

$$v = \pm\left(v_0{}^2 + \left[6(1+\Delta^3)\epsilon_1\epsilon_2\cos\varphi\right](\omega R_{01})^2\left(\frac{1}{x}-\frac{1}{x_0}\right)\right)^{1/2}. \tag{45}$$

The particular case of equal-size bubbles, starting their approach from relative rest ($v_0 \to 0$), at very large separations ($x_0 \to \infty$) is of special interest for further studies:

$$v_{s1} = -2\sqrt{3}\frac{\epsilon}{x^{1/2}}\omega R_0. \tag{46}$$

Substituting (6) in (46) leads to

$$v_{s1} = -2\sqrt{3}\frac{\theta(q)}{x^{1/2}}\frac{A}{\rho\omega R_0}. \tag{47}$$

The function $\theta(q)$ has a maximum at $q_0 = 1/(1-2\delta^2)$. Further analysis of (47) shows that a pair of equal-size bubbles will reach a higher relative velocity at the same distance x if their frequency index q has a value near q_0. Figure 6 presents $v_{s1}(x)$ in the case of two equal-size bubbles in water at 20 °C, driven at 22.5 kHz with a forcing amplitude of $A = 50$ kPa and for various sizes R_0.

3.2.4. *Analytic solutions*

Assume that for a pair of non-resonant bubbles the initial conditions are given such that the total energy E is fixed. The derivative $\mathrm{d}\tau/\mathrm{d}\xi$ is obtained from equation (41):

$$\frac{\mathrm{d}\tau}{\mathrm{d}\xi} = \pm\left(\frac{\xi}{E\xi+1}\right)^{1/2}. \tag{48}$$

Although a general quadrature is possible (and it will be performed later), two limiting values for E are investigated initially:

(*a*) $E = 0$. With this assumption, equation (48) is integrated and the result can be inverted to

$$\xi(\tau) = \left({\xi_0}^{3/2} \pm \tfrac{3}{2}\tau\right)^{2/3}. \tag{49}$$

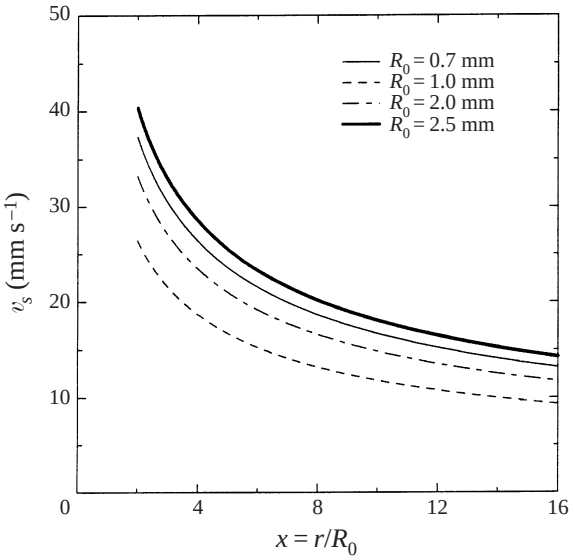

FIGURE 6. Variation with distance of the relative velocity: two equal bubbles starting at large separations.

(*b*) $E \to \infty$. Physically, this limiting case corresponds to very large initial relative velocities, since the potential energy has a finite maximum value at $\xi_{lim} \neq 0$. The right-hand side of equation (48) is approximated with $\pm 1/E^{1/2}$, resulting in

$$\xi(\tau) = \xi_0 \pm \frac{1}{E^{1/2}}\tau. \tag{50}$$

When E is different from these limiting values, equation (48) is integrated to

$$f(\xi) = f(\xi_0) \pm \tau. \tag{51}$$

Equation (51) is, in general, too complicated to be inverted to $\xi = \xi(\tau)$ as above. The form of the function $f(\xi)$ is different when the sign of the total energy function is plus or minus:

$E > 0$:

$$f(\xi) = \frac{1}{E}\left((\xi(E\xi + 1))^{1/2} + \frac{1}{2E^{1/2}} \ln \left| \frac{(E + 1/\xi)^{1/2} - E^{1/2}}{E^{1/2} + (E + 1/\xi)^{1/2}} \right| \right); \tag{52}$$

$E < 0$:

$$f(\xi) = \frac{1}{E}\left((\xi(E\xi + 1))^{1/2} - \frac{1}{E} \arctan \frac{1}{|E|} \left(\frac{\xi}{E\xi + 1} \right)^{1/2} \right). \tag{53}$$

3.3. *Dynamics of a resonant pair of bubbles*

As mentioned in § 2.6, only the cases of resonant pairs of bubbles satisfying the additional condition

$$\epsilon_{1\infty}\epsilon_2 < \cos\varphi < 2\epsilon_{1\infty}\epsilon_2 \tag{54}$$

are considered. This condition is also necessary for the existence of a stable equilibrium separation. The sign of the interaction forces changes from positive (repulsion at smaller distances) to negative (attraction at larger distances) when the bubbles are at this separation distance. A direct numerical analysis of different pairs of resonant

bubbles, driven at low forcing amplitude, shows that the two bubbles must have nearly equal radii in order to satisfy the condition expressed in (54). Therefore, the size ratio must be close to one: $\Delta \approx 1$. The admissible range for Δ, to obtain a resonant pair which satisfies (54), is wider around 1 as the forcing amplitude A is increased. The equation of motion is (30), with the attraction coefficient $\mathscr{K}$ given by (33) and the repulsion coefficient $\mathscr{B}$ given by (34). The mathematical space to be used is defined by the new variables (τ, ξ):

$$\xi \equiv \gamma x, \tag{55}$$

$$\tau \equiv \tilde{\mathscr{B}} \gamma^2 \tilde{t}, \tag{56}$$

where the scaling parameter

$$\gamma \equiv \frac{\mathscr{K}}{\mathscr{B}}, \tag{57}$$

is the ratio between the attraction and the repulsion coefficients in the interaction forces. The study of the relative motion of a pair of resonant bubbles is reduced to the study of nonlinear ODE

$$\frac{\mathrm{d}^2\xi}{\mathrm{d}\tau^2} = \frac{1}{2}\left[-\frac{1}{\xi^2} + \frac{2}{\xi^3}\right]. \tag{58}$$

A canonical form of the dynamical system is derived from equation (58):

$$\frac{\mathrm{d}w}{\mathrm{d}\tau} = \frac{1}{2}\left[-\frac{1}{\xi^2} + \frac{2}{\xi^3}\right], \quad \frac{\mathrm{d}\xi}{\mathrm{d}\tau} = w. \tag{59}$$

In this case, the potential function has the form $U(\xi) \equiv -1/\xi + 1/\xi^2$. The total energy is defined as $E(\xi, w) \equiv U(\xi) + w^2$ and it is constant throughout the motion, determined by the initial conditions of the problem (ξ_0, w_0).

Figure 3 presents the potential function of a resonant pair as a solid line. Since condition (54) was assumed true, only the positive domain for ξ has to be studied. The graph shows the existence of a minimum point for $U(\xi)$ in the positive domain for ξ, which implies the existence of a stable equilibrium value for the separation distance. Figure 3 contains also, as a dot-dashed line, the potential of an anti-resonant pair of bubbles for $\cos\varphi < \epsilon_{1\infty}\epsilon_2$, when a maximum for $U(\xi)$ in the positive-ξ domain is present; thus an unstable equilibrium value for the distance may occur. A simple study of $U(\xi)$ provides (i) a zero at $\xi = 1$; (ii) zero limit for $\xi \to \infty$; (iii) a minimum point at $\xi_r = 2$, where $U_{min} = -\frac{1}{4}$ (i.e. the interaction forces are zero); and (iv) an inflection point at $\xi_a = 3$, where the attraction forces have a local maximum. The total energy function $E(\xi, w) = U(\xi) + w^2$ can have only values greater than $E_{min} = -\frac{1}{4}$, which corresponds to a state of stable equilibrium at rest, for $\xi_r = 2$.

Figure 7 shows the possible trajectories of the system in the phase plane (ξ, w) for different total energies E, and in the positive semiplane $\xi > 0$. The graph is based on the relation

$$w = \pm\frac{(E\xi^2 + \xi - 1)^{1/2}}{\xi}. \tag{60}$$

The thick vertical line designates the collision condition $\xi_{lim} = \gamma(1 + \Delta) \approx 2\gamma$.

3.3.1. *Negative total energy*

Consider the equation

$$w = 0 \Leftrightarrow E\xi^2 + \xi - 1 = 0. \tag{61}$$

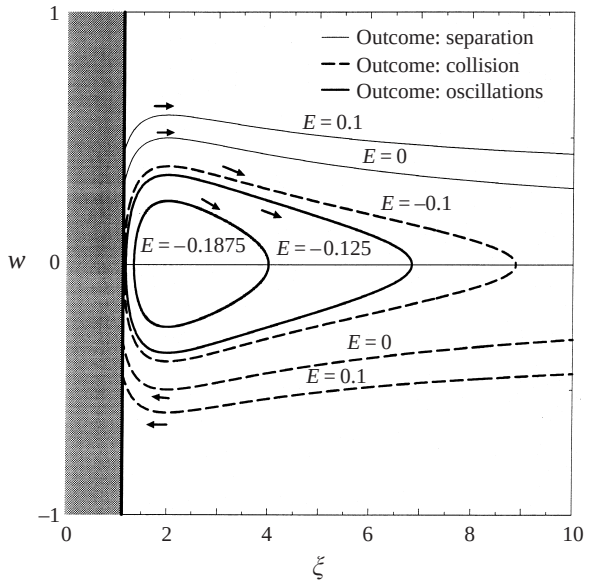

FIGURE 7. Trajectories in the phase plane for the relative motion of a pair of resonant bubbles.

A simple root analysis shows that equation (61) has two positive roots, ξ_1 and ξ_2, for any possible negative value of the total energy. The product and the sum of the roots are both equal to the positive quantity $-1/E$. The evolution of the system is bounded by these two values $\xi_2 < \xi_1$, and the trajectory is a closed curve in the phase plane. Hence, a periodic motion (translational oscillations) may occur. However, if the smaller root ξ_2 is less than ξ_{lim}, then the two bubbles will collide during the first cycle of the oscillations. With the approximation $\Delta \approx 1$, the condition for such a collision is written as

$$E > \frac{1-2\gamma}{4\gamma^2}. \tag{62}$$

Combining (62) with the assumed case $-\frac{1}{4} < E < 0$, the motion of a given pair of resonant bubbles (γ is fixed) can be predicted if the initial conditions (E) are known.

(*a*) If $0 < \gamma < \frac{1}{2}$ and $-\frac{1}{4} < E < 0$, repulsion forces are strong enough to maintain the two bubbles separated in a periodic motion between the limits

$$\xi_1 = -\frac{1+(1+4E)^{1/2}}{2E} \tag{63}$$

and

$$\xi_2 = -\frac{1-(1+4E)^{1/2}}{2E}. \tag{64}$$

The equilibrium value is $\xi_r = 2$. Two amplitudes, α_1 and α_2, can be defined with respect to this ξ_r:

$$\alpha_{1,2} \equiv \xi_{1,2} - \xi_r = -\frac{(1+4E)^{1/2}(1 \pm (1+4E)^{1/2})}{2E}. \tag{65}$$

Only in the particular case of $E = -\frac{1}{4}$ (stable equilibrium at rest), are the two amplitudes both equal to 0, otherwise they have different values. Their sum is $2\alpha \equiv \alpha_1 + \alpha_2 = -(1+4E)^{1/2}/E$ and gives the amplitude X for this periodic motion: $2X \equiv 2\alpha/\gamma$. Sub-

stituting γ back into physical quantities:

$$2X = \Delta\theta(q_2)\left(\frac{2\epsilon_{1\infty}\epsilon_2 - \cos\varphi}{\cos\varphi - \epsilon_{1\infty}\epsilon_2}\right)\left(\frac{1}{4|E|^2} - \frac{1}{|E|}\right)^{1/2}. \tag{66}$$

Equation (66) shows that the amplitude of oscillations depends on the characteristics of each bubble pulsation $(\varphi, \epsilon_i, q_2)$, on the bubble size ratio Δ, and unlike the linear oscillator, on the initial conditions, through the total energy E.

(*b*) If $\frac{1}{2} < \gamma < 1$ and $-\frac{1}{4} < E < (1-2\gamma)/(4\gamma^2)$, again a periodic motion between ξ_2 and ξ_1 is maintained. Relations (63)–(65) remain valid.

(*c*) If $\frac{1}{2} < \gamma < 1$ and $(1-2\gamma)/(4\gamma^2) < E < 0$, the two bubbles collide during the first cycle of the periodic motion imposed in these conditions.

(*d*) If $\gamma \geqslant 1$, repulsion forces at small distances are not strong enough to consume the kinetic energy acquired in the approach motion and collision occurs for any $-\frac{1}{4} < E < 0$, during the first cycle of the oscillation. In the phase plane (ξ, w) this subcase corresponds to having the limiting line to the right of the point $\xi_r = 2$.

3.3.2. *Positive total energy*

In this case, the equation $E\xi^2 + \xi - 1 = 0$ has a positive root $\xi_1 = ((1+4E)^{1/2} - 1)/(2E)$ and a negative one $\xi_2 = -((1+4E)^{1/2} + 1)/(2E)$. The only possible values for bubble spacing are $\xi > \xi_1 > 0$. The trajectories in the phase plane (ξ, w) show that for an initial approach motion the two bubbles have enough kinetic energy to overcome the repulsion forces and the motion ends with their collision. For an initial separation motion the kinetic energy is enough to overcome the net attraction force at large distances and the bubbles continue to separate toward an infinite distance. The value of the attraction/repulsion scaling coefficient γ determines if the relative velocity has a maximum absolute value during the motion (during both approach and separation patterns). The following cases are considered.

(*a*) If $0 < \gamma \leqslant 1$, $|v|$ has a maximum $|v|_r$ for $\xi = \xi_r$, when the potential energy is minimum.

$$|w|_r = (E + U_{min})^{1/2} = \frac{(4E+1)^{1/2}}{2}. \tag{67}$$

Substituting back in the dimensional relative velocity:

$$|v|_r = \left(\frac{3\left(1+\Delta^{-3}\right)(4E+1)}{2\epsilon_{1\infty}\epsilon_2 - \cos\varphi}\right)^{1/2}(\cos\varphi - \epsilon_{1\infty}\epsilon_2)\frac{A}{\rho\omega R_{01}}. \tag{68}$$

After the distance becomes larger or smaller than ξ_r, the two bubbles move towards collision or towards infinite separation at relative velocities smaller than $|v|_r$.

(*b*) If $\gamma > 1$, relative velocity continuously increases as the two bubbles approach each other and, respectively, decreases continuously as they move away from each other.

3.3.3. *Analytic solutions*

A general analytic relation between time and bubbles spacing is found starting with the differential equation

$$\frac{\mathrm{d}\tau}{\mathrm{d}\xi} = \pm\frac{\xi}{(E\xi^2 + \xi - 1)^{1/2}}. \tag{69}$$

There are two limiting cases with respect to the total energy:

(*a*) $E = 0$. The class of initial conditions (x_0, v_0) which correspond to zero total energy is described by

$$|v|_0 = \left(6(1+\Delta^3)\epsilon_{1\infty}\epsilon_2(\cos\varphi - \epsilon_{1\infty}\epsilon_2)\frac{1}{x_0}\left(1-\frac{1}{\gamma x_0}\right)\right)^{1/2}\omega R_{01}. \tag{70}$$

In this particular case, the two roots are equal, $\xi_1 = \xi_2 = 1$, and a relatively simple relation of the type

$$g(\xi) = g(\xi_0) \pm \tau \tag{71}$$

is obtained through direct integration of (69), where

$$g(\xi) = \tfrac{2}{3}(\xi+2)(\xi-1)^{1/2}. \tag{72}$$

(*b*) $E \to \infty$. The solution is the same as the solution derived for a non-resonant pair at high energies:

$$\xi(\tau) = \xi_0 \pm \frac{1}{E^{1/2}}\tau. \tag{73}$$

The explanation for obtaining the same solution resides in the fact that for large initial velocities (large E), Bjerknes secondary forces have a small effect on the variation of relative velocity.

For finite non-zero values of the total energy function, the above approximations are not valid and (69) is integrated in the general form, which allows only for an implicit study of $\xi(\tau)$:

$$h(\xi) = h(\xi_0) \pm \tau. \tag{74}$$

The function $h(\xi)$ has different forms for negative or positive total energy:

$E > 0$, $\xi > \xi_1 > 0$:

$$h(\xi) = \frac{1}{4E}\ln\left(2\xi - 2\left(\xi^2 + \frac{1}{E}\xi - 1\right)^{1/2} + \frac{1}{E}\right) + \frac{1}{2}\left(\xi^2 + \frac{1}{E}\xi - 1\right)^{1/2}; \tag{75}$$

$E < 0$, $0 < \xi_2 < \xi < \xi_1$ (the roots ξ_1, ξ_2 are given by equations (63)–(64)):

$$h(\xi) = \frac{1}{|E|}\left[\frac{1}{|E|^{1/2}}\ \arctan\left(\frac{\xi-\xi_2}{\xi_1-\xi}\right)^{1/2} - (E\xi^2+\xi-1)^{1/2}\right]. \tag{76}$$

When $\xi \to \xi_1$ (maximum separation distance between the bubbles), the second term in $h(\xi)$ can be neglected, since

$$\lim_{\xi \nearrow \xi_1}(E\xi^2+\xi-1)^{1/2} = 0,$$

$$\lim_{\xi \nearrow \xi_1}\ \arctan\left(\frac{\xi-\xi_2}{\xi_1-\xi}\right)^{1/2} = \frac{\pi}{2}.$$

The first term on the right-hand side of equation (76) can be easily inverted and an explicit relation for $\xi = \xi(\tau)$ is obtained:

$$\xi(\tau) \approx \frac{\xi_2 + \xi_1 \tan^2 c\tau}{1 + \tan^2 c\tau}, \tag{77}$$

where $c \equiv |E|^{3/2}$. An equivalent form for $h(\xi)$ can be derived through the integration of equation (69):

$$h(\xi) = -\frac{1}{|E|}\left[\frac{1}{|E|^{1/2}}\ \arctan\left(\frac{\xi_1-\xi}{\xi-\xi_2}\right)^{1/2} + (E\xi^2+\xi-1)^{1/2}\right]. \tag{78}$$

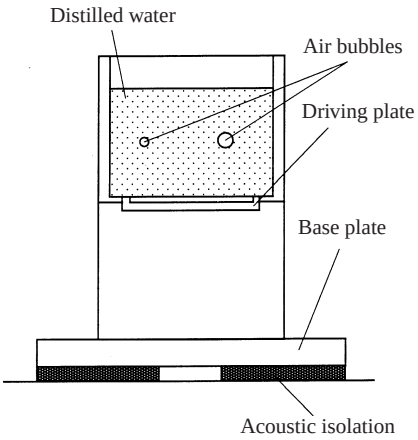

FIGURE 8. Acoustic levitator.

This form is used to derive an explicit relation for $\xi = \xi(\tau)$ when $\xi \to \xi_2$ (minimum separation distance between the bubbles):

$$\xi(\tau) \approx \frac{\xi_1 + \xi_2 \tan^2 c\tau}{1 + \tan^2 c\tau}. \tag{79}$$

The two limits of relation $\xi = \xi(\tau)$, (77) and (79), provide the period $\mathscr{T}$ of the oscillatory pattern of two resonant bubbles:

$$\mathscr{T} \approx \frac{\pi}{c} = \pi |E|^{-3/2}. \tag{80}$$

An exact value for this important time scale cannot be obtained from the general relation (74), due to the complicated form of the function $h(\xi)$. However, the approximate value (80) can be very useful in estimating the frequency of the translational oscillations, v, defined as $v \equiv A/\rho\omega R_{01}^2 \cdot \tilde{b}\gamma^2/\mathscr{T}$, or after substitution:

$$v \approx \frac{4}{\pi}\theta(q_2)\left(\frac{\cos\varphi - \epsilon_{1\infty}\epsilon_2}{2\epsilon_{1\infty}\epsilon_2 - \cos\varphi}\right)^2 \left(3\left(\Delta^2 + \frac{1}{\Delta}\right)\epsilon_{1\infty}(2\epsilon_{1\infty}\epsilon_2 - \cos\varphi)\right)^{1/2} \times |E|^{3/2}\left(\frac{A}{\rho R_{01}^2}\right)^{1/2}. \tag{81}$$

For a known forcing (A, f) and a given pair of resonant bubbles $(\varphi, \epsilon_i, q_2, R_{0i}, \Delta)$, the oscillation frequency varies with the initial conditions of the motion, through the value of the total energy $E(\xi_0, w_0)$.

4. Experiments

4.1. *Experimental setup*

Since the oscillating type of bubble–bubble interaction has not been reported earlier, we have conducted our own experiments to support the theoretical findings. In the following subsections, the experimental apparatus is described along with the measurement procedures, and the experimental findings are presented in comparison with the theoretical predictions.

Figure 8 is a schematic representation of the acoustic levitator. This levitator

consists of a tank with transparent walls of dimensions ($11 \times 11 \times 8$ cm), designed such that stationary sound waves can be obtained at applied frequencies of 20–25 kHz. The acoustic field is produced by a thin-wall hollow-cylinder piezoceramic transducer whose resonance frequency is 22.5 kHz. For this frequency, the level of distilled water inside the tank which ensures a stable levitation of the bubbles is 63 mm. The maximum radius of a levitated air bubble is 3.5 mm. The sinusoidal signal is generated by a Hewlett–Packard 33120A Function Generator and amplified by a Hewlett–Packard 6824A Amplifier. The signal is checked with a Gould 4050 Oscilloscope at the exit of the amplifier for any distortions.

A stationary sound wave is formed inside the tank with its minimum pressure plane located approximatively at the middle of the water depth. The air bubbles are levitated at this location. Bubble pairs with different initial distances are tested. The position of each bubble is accurately determined with an Edmund Scientific laser pointer ML-211 and a graded transparent grid. Their motion is recorded and then analysed using a Kodak EktaPro 1000 Motion Analyzer, choosing the rate (frames/second) between 60 and 1000, and adjusting the magnification on the screen with the Chinon-Hoya Zoom System.

The acoustic pressure distribution inside the tank is measured using a small hydrophone (3 mm in diameter), the oscilloscope and its attached Gould Waveform Processor 150. More than 300 points at three levels inside the tank are used to map the amplitude of the sound field. In addition, the flow field around the bubbles has been investigated with dye techniques and found to be insignificant. Therefore, the only cause of the relative motion of the pair of bubbles is their secondary Bjerknes interaction.

In a typical experiment, two air bubbles of different radii are manually injected by an hypodermic needle at different separation distances and their motion is recorded and played back frame-by-frame. The reticle provided by the EktaPro system is used to determine the radius and the location of the centre of mass for each bubble. The motion of the pair is studied only after the initial vertical motion due to the injection has died down. The applied frequency is kept constant at 22.5 kHz. At this high frequency, we were unable to measure with accuracy the amplitude of the volume oscillations of the bubbles. Therefore, this quantity is determined indirectly by balancing the buoyancy and primary Bjerknes forces on each bubble (Eller 1968).

4.2. *Principal patterns of interaction*

There are two principal patterns of interaction observed in the experiments.

(i) Pairs of large bubbles (radius between 0.5 mm and 3 mm) show mutual attraction leading to collision and coalescence. Figure 9 presents photos of video frames of this kind of interaction.

(ii) Pairs of small bubbles (radius around 0.15 mm) display an oscillatory motion along their line of centres.

4.2.1. *Attraction/collision*

Figure 10 presents bubble spacing as a function of time for several experiments in which the outcome was the collision of bubbles. The distance between the centres of the two bubbles is normalized with the initial distance r_0 and the time is normalized with the time scale r_0/v_0, derived from a uniform relative motion started with v_0. The amplitude of the forcing and the radii of the bubbles are indicated in table 1; the forcing frequency is 22.5 kHz for all four experiments. Table 1 also contains experimental information concerning the initial bubble spacing and velocity. The first

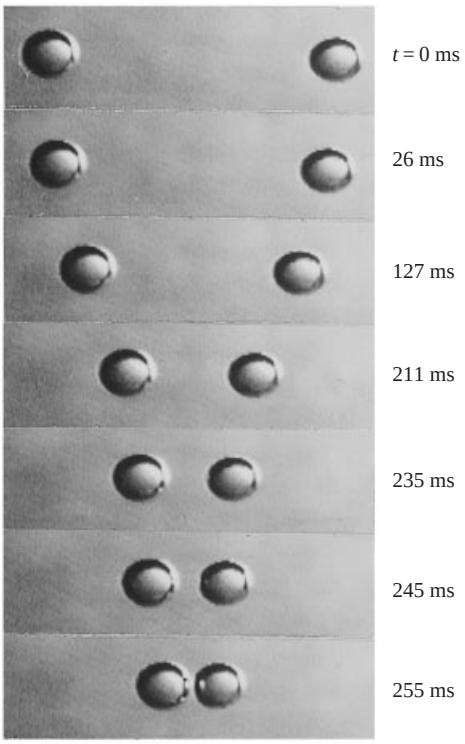

FIGURE 9. One-dimensional relative dynamics of two attracting bubbles.

Experiment	R_{01} (mm)	R_{02} (mm)	A (kPa)	r_0 (mm)	v_0 (mm s^{-1})
A	2.402	1.952	33	42.79	18.9
B	1.583	1.417	21	28.67	26.3
C	1.661	0.779	18	12.82	42.3
D	1.546	1.289	15	26.55	43.7

TABLE 1. Experimental data–pairs of attracting bubbles.

stage of the relative motion of two bubbles is characterized by the dominant effect of the initial kinetic energy, such that v_0 is almost unchanged. This stage lasts longer for large initial velocities and small forcing amplitudes (experiment D). The second stage of the relative motion is characterized by the increasing acceleration induced by the interaction between the bubbles. The larger is the forcing amplitude, the higher are the accelerations towards the collision of the bubbles, as indicated by the changes in the slope of the experimental curves: A > B > C > D.

The velocities of the bubbles are computed based on their recorded locations, using a numerical differentiation procedure with unequal time steps. Figure 11 presents the variation of relative velocity $v = v_2 - v_1$ with the distance $r = r_2 - r_1$ between the bubbles, for both experimental (symbols) and theoretical predictions (lines). The two sets of curves are similar; however, the conservative model, which does not consider the drag forces, over-predicts the values for the relative velocity. The differences between the theoretical and the experimental values increase as the motion proceeds and the

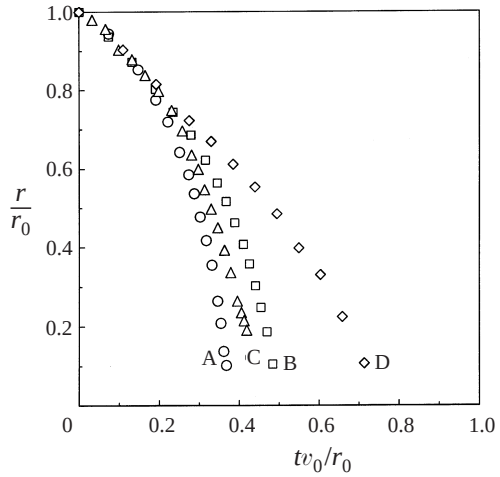

FIGURE 10. History of the locations of each bubble.

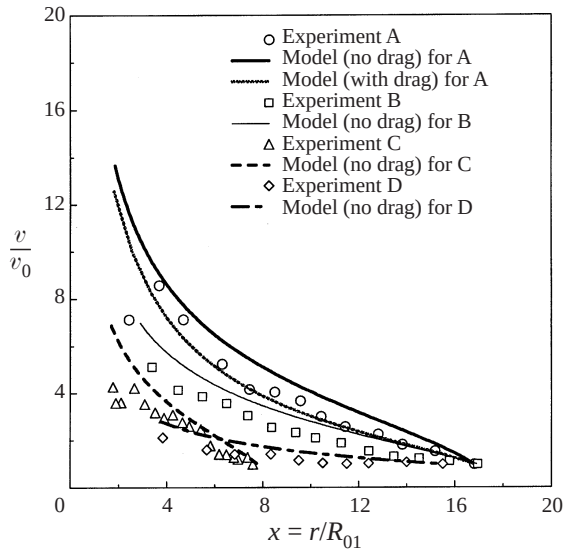

FIGURE 11. Relative velocity of the bubbles: variation with distance apart.

separation distance decreases. They are significant especially after the separation of the two interfaces becomes smaller than 3 radii, when both the drag effects and the coupling between the bubble pulsations have significant influence upon the motion.

4.2.2. *Oscillations*

Figure 12 shows the experimental data obtained from the interaction of two bubbles, practically of the same size (radii of 0.146 and 0.137 mm). For this bubble size, the resonance frequency for pure radial volume oscillations is 22.482 and 23.972 kHz, respectively (both close to the applied frequency of 22.5 kHz). The frequency indices of this pair of bubbles are $q_1 = 1.00079$ and $q_2 = 0.93861$. The forcing amplitude is small compared with previous experiments (where levitation of larger bubbles was required), $A = 1.35$ kPa. The locations of the bubbles show a cyclic motion, featuring

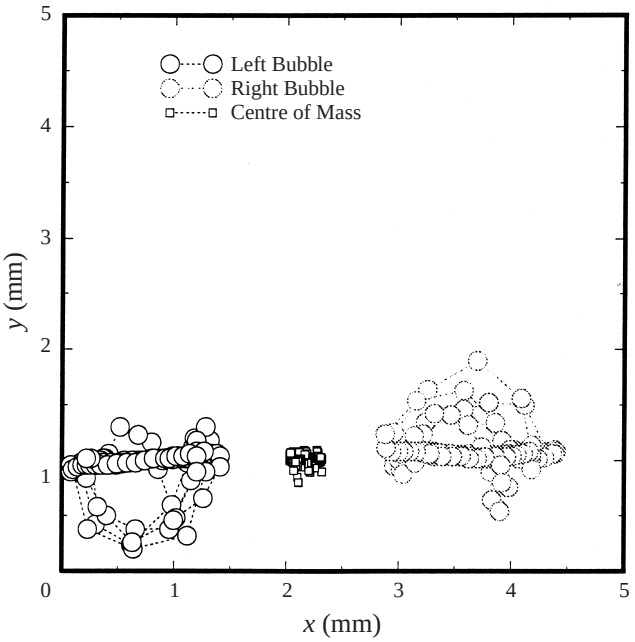

FIGURE 12. Cyclic motion of a pair of bubbles driven close to their resonance frequencies.

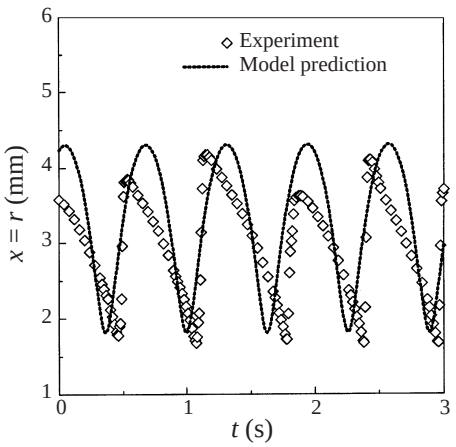

FIGURE 13. Experimental data for oscillations in the x-direction and theoretical predictions for this one-dimensional periodic motion.

a slow approach stage along the horizontal x-direction and a violent repulsion which takes the bubbles out of the equilibrium plane. In the repulsion stage the bubbles go through considerable shape deformations due to large accelerations.

Figure 13 presents the history of these translational oscillations in the x-direction only, by showing the variation in time of the separation distance between their centres. The vertical y-motion is influenced by the action of the primary Bjerknes forces and thus must be separated from the effects of the smaller secondary Bjerknes forces. Figure 13 presents five cycles of the motion, lasting 3 s, which correspond to a frequency of 1.67 Hz. The oscillations of the distance between the centres are bounded by a minimum value of 14 radii and a maximum one of 29 radii. The

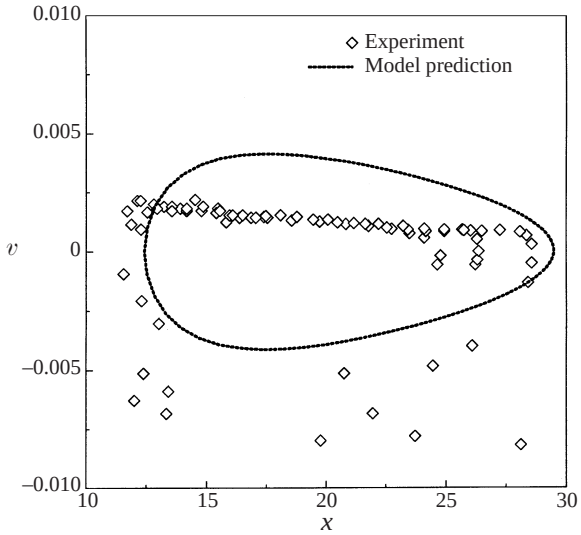

FIGURE 14. Relative velocity of oscillation: variation with distance apart.

theoretical predictions of the proposed model for the corresponding resonant pair of bubbles engaged in oscillatory motion are also presented in figure 13 for comparison. Theoretical values predicted for the oscillatory mode of relative motion are frequency 1.58 Hz, minimum separation at 12.4 radii, maximum separation at 29.5 radii, in good agreement with the experimental values. However, the difference between the history of motion recorded by the experiment and the history predicted by the conservative model is significant for the relative velocity. The separation motion features relative velocities six to eight times higher than the approach stage. This 'hysteresis' in relative velocity is not predicted by the theory. An explanation for this phenomenon may be the fact that the separation motion starts at smaller bubble spacings, with much larger accelerations generated by the term proportional to r^{-3} in the interaction field. This fact triggers, especially for the coupled oscillations of a resonant pair of bubbles, shape oscillations and a significant departure from the spherical shape assumed in the derivation of the model. Therefore, during the separation phase, spherical-cap and star-like shapes, and even tiny breakups of the bubbles are observed. This is the first experimental observation which verifies the computational work by Pelekasis & Tsamopoulos (1993*a*, *b*), regarding the spherical-cap and star-like shapes of increasingly accelerated interacting bubbles. As the separation motion slows down after the sign change in the interaction field, and under the damping effect of the liquid viscosity (drag forces), the bubbles regain their spherical shape and the motion turns smoothly to approach, at large bubble spacings, under the influence of the r^{-2} term.

Figure 14 shows the variation of the relative velocity with the separation distance r. Theoretical prediction of $v(r)$, given by our conservative model (the dotted line) is inserted for comparison with the experimentally deduced velocity (the diamonds). The spread of the experimental data is attributed to the variations in the instantaneous levitation depth of each bubble. In other words, the bubbles do not move exactly in one horizontal plane. There is a slight three-dimensionality in the flow pattern, which may explain the spread in the data. The loss of spherical shape explains the y-motion, since for distorted shapes of the bubble, the levitation force (primary Bjerknes force) can be higher or lower than the gravitational buoyancy.

Pair type	Non-resonant		Resonant
Phase shifts φ_i	$0 \leqslant \varphi_1, \varphi_2 \ll \pi/2$ or $\pi/2 \ll \varphi_1, \varphi_2 \leqslant \pi$	$0 \leqslant \varphi_1 \ll \pi/2$ and $\pi/2 \ll \varphi_2 \leqslant \pi$	$\pi/2 \ll \varphi_1 \leqslant \pi$ and $\varphi_2 \to \pi/2$
Interaction force	$-a/r^2$	a/r^2	$-a/r^2 + b/r^3$
Effect	Attraction	Repulsion	Stable equilibrium point

TABLE 2. Classification of the binary systems of bubbles.

5. Summary and conclusions

The dynamic patterns of a pair of interacting bubbles are determined by the characteristics of the responses of the two interfaces to the forcing sound wave. While previous linear theory of secondary Bjerknes forces used an undamped model for the radial oscillations of the bubbles, our approach considers viscous, thermal and acoustic damping effects in bubble pulsations.

The frequency index of each bubble (q), defined as the ratio of the forcing frequency to the resonance frequency of the bubble, is the governing parameter for the values of the phase shifts φ_i and response amplitudes ϵ_i. A bubble with $q < 1$ is driven below its resonance frequency. This bubble oscillates out of phase with respect to the forcing wave and its emitted secondary pressure field increases the amplitude of the primary pressure field. A bubble with $q > 1$ is driven above its resonance frequency. This bubble oscillates in phase with the forcing and its emitted secondary pressure field decreases the amplitude of the primary pressure field. Table 2 summarizes the classification of the binary systems of bubbles based upon their values of frequency indices. The new model proposed in our paper reduces to the previous linear theories for non-resonant pairs of bubbles. For this category, there is no coupling effect considered between the two oscillators. The other two classes of bubble pairs, namely resonant and anti-resonant, show significant coupling effects. The response amplitude of the bubble driven close to resonance varies with the separation distance. This variation is implemented in the general formula for the secondary Bjerknes forces, resulting in a new mathematical description of the interaction force field. Beside the r^{-2} term, a term proportional to r^{-3} appears in the new formula for the interaction force. As a result, a sign change may appear for the interaction force, and a new pattern of relative motion is possible: the oscillations of the two bubbles along their line of centres, around a stable equilibrium position.

The non-resonant pairs of bubbles show only two patterns of interaction: attraction and repulsion. However, the outcomes of such interactions may depend on the initial conditions (separation and relative velocity), through the value of the total energy E. Tables 3(a) and 3(b) provide this dependence for attracting and repelling non-resonant bubbles, respectively. In table 3(a), the escape velocity, $\hat{v}_e$, is defined as the initial relative separation velocity necessary for two attracting bubbles to overcome the effect of their attraction and separate an infinite distance (scatter):

$$\hat{v}_e = \left(6(1 + \Delta^3)\,\epsilon_1\epsilon_2 \cos\varphi\right)^{1/2} \frac{1}{x_0^{1/2}}\,\omega R_{01}. \tag{82}$$

The collision velocity, v_m, is defined as the initial relative approach velocity necessary

	Energy level	Initial relative velocity	Outcome of interaction
(*a*)	$E < 0$	$-\hat{v}_e < v_0 < \hat{v}_e$	Collision
	$E = 0$	$v_0 = \hat{v}_e$	Scattering, $v_\infty = 0$
	$E > 0$	$v_0 > \hat{v}_e$	Scattering, $v_\infty > 0$
	$E > 0$	$v_0 < -\hat{v}_e$	Collision
(*b*)	$E > 0$	$-v_m < v_0$	Scattering, $v_\infty > 0$
	$E = E_m > 0$	$v_0 = -v_m$	Scattering, $v_\infty = 0$
	$E > E_m > 0$	$v_0 < -v_m < 0$	Collision

TABLE 3. Outcomes of interaction for non-resonant (*a*) attracting bubbles and (*b*) repelling bubbles.

for two bubbles to collide at zero velocity, although they repel each other:

$$v_m = \left(6\epsilon_1\epsilon_2 \cos\varphi \left[-\left(1-\frac{1}{x_0}\right) + \Delta - \Delta^2 + \frac{1}{x_0}\Delta^3\right]\right)^{1/2} \omega R_{01}. \tag{83}$$

The particular case of two equal-size bubbles, always attracting each other, is analysed separately in order to understand the influence of the other parameters of the problem. The relative velocity of two equal-size bubbles, interacting through secondary Bjerknes forces, is found to be proportional to their size, the response amplitude and the forcing frequency, and inversely proportional to the square root of the separation distance. The relative velocity has a maximum value at $q_0 = 1/(1-2\delta^2)$, a value slightly higher than the resonance value 1, depending on the damping coefficient at bubble interface δ.

The resonant pairs of bubbles may show a sign change in the interaction force, from attraction at large distances to repulsion at small distances, featuring a stable equilibrium point. The anti-resonant pairs may show a reverse sign change in secondary Bjerknes forces, from repulsion at large distances to attraction at small distances, featuring an unstable equilibrium point. The ratio of attraction to repulsion coefficients in the new formula for the interaction force, γ, and the total energy, E, are the parameters which govern the outcomes of the relative motion for a resonant/anti-resonant pair of bubbles. Table 4 contains a complete description of the patterns of motion and the outcomes for a resonant pair of bubbles for various scaling parameters γ and total energy E. The limiting values for the initial relative velocity are in this case v_e, defined by the condition $E = 0$, and v_p, defined by the condition of collision at zero velocity:

$$v_e \equiv \left(6(1+\Delta^3)\epsilon_{1\infty}\epsilon_2(\cos\varphi - \epsilon_{1\infty}\epsilon_2)\frac{1}{x_0}\left(1-\frac{1}{\gamma x_0}\right)\right)^{1/2} \omega R_{01}, \tag{84}$$

and

$$v_p \equiv \left(\frac{\gamma x_0 - 1}{{x_0}^2} + \frac{1-2\gamma}{4}\right)^{1/2} \left(3\Delta(1+\Delta^3)\theta(q_2)\epsilon_{1\infty}\epsilon_2^2(2\epsilon_{1\infty}\epsilon_2 - \cos\varphi)\right)^{1/2} \omega R_{01}. \tag{85}$$

An analysis of tables 2 and 3, focusing on the outcome of interaction, rather than on the sign of the interaction forces, can be summarized as follows.

1. Non-resonant pairs of bubbles, characterized by $\gamma \to \infty$ (since there is no repulsion term), evolve toward collision or scattering. Low-energy non-resonant pairs will collide or scatter, in the sense determined by the interaction force. High-energy

γ	Energy level	Initial relative velocity	Relative velocity variation	Outcome of interaction
$\gamma < 1/2$	$E < 0$	$-v_e < v_0 < v_e$	Periodic	Oscillations
$\gamma < 1/2$	$E = 0$	$v_0 = -v_e$	v has a maximum before collision	Collision
$\gamma < 1/2$	$E = 0$	$v_0 = v_e$	v has a maximum at finite separation	Scattering at $v_\infty = 0$
$\gamma < 1/2$	$E > 0$	$v_0 < -v_e$	v has a maximum before collision	Collision
$\gamma < 1/2$	$E > 0$	$v_0 > v_e$	v has a maximum at finite separation	Scattering at $v_\infty > 0$
$\frac{1}{2} < \gamma < 1$	$E < E_p$	$-v_p < v_0 < v_p$	Periodic	Oscillations
$\frac{1}{2} < \gamma < 1$	$E_p < E < 0$	$-v_e < v_0 < -v_p$ or $v_p < v_0 < v_e$	Collision during the second half of the first cycle	Collision
$\frac{1}{2} < \gamma < 1$	$E = 0$	$v_0 = -v_e$	v has a maximum before collision	Collision
$\frac{1}{2} < \gamma < 1$	$E = 0$	$v_0 = v_e$	v has a maximum at finite separation	Scattering at $v_\infty = 0$
$\frac{1}{2} < \gamma < 1$	$E > 0$	$v_0 < -v_e$	v has a maximum before collision	Collision
$\frac{1}{2} < \gamma < 1$	$E > 0$	$v_0 > v_e$	v has a maximum at finite separation	Scattering at $v_\infty > 0$
$1 < \gamma$	$E < 0$	$-v_e < v_0 < v_e$	Collision during the first half of the first cycle	Collision
$1 < \gamma$	$E = 0$	$v_0 = -v_e$	v increases to collision	Collision
$1 < \gamma$	$E = 0$	$v_0 = v_e$	v decreases towards v_∞	Scattering at $v_\infty = 0$
$1 < \gamma$	$E > 0$	$v_0 < -v_e$	v increases to collision	Collision
$1 < \gamma$	$E > 0$	$v_0 > v_e$	v decreases towards v_∞	Scattering at $v_\infty > 0$

TABLE 4. Outcomes of interaction for a pair of resonant bubbles.

pairs, moving initially in the opposite sense with the interaction force, will result in collisions of repelling bubbles and respectively, scattering of attracting bubbles.

2. Resonant pairs of bubbles with $\gamma > 1$ behave same as the non-resonant pairs; only the magnitudes of the limiting conditions are different.

3. Resonant pairs of bubbles with $0 < \gamma < \frac{1}{2}$ or with $\frac{1}{2} < \gamma < 1$ present a new feature with respect to the above categories: intermediate-energy pairs maintain a periodic relative motion. The period and the amplitude, of these nonlinear oscillations are determined in our theory as functions of the forcing amplitude, the forcing frequency, and the total energy.

The theoretical findings are verified by experimental studies. The experimental findings reinforce the previous studies with new data about the attraction motion of two levitated bubbles, both driven above their resonance frequency, starting at relatively large distances. The relative velocity profile obtained experimentally is compared with the analytic solution. There is a good agreement between the analytic

solution and the experimental results for large bubble separations. However, when the two bubbles are close, i.e. the distance between their centres is less than 3–4 radii, the effect of the drag forces, which are not considered in the conservative model used to derive the analytic solution, becomes significant, and the theory over-predicts the relative velocity near the collision moment by a factor of 1.5–2. The existence of the translational oscillations of the two bubbles along their line of centres, predicted by the new model, is verified by experiments involving pairs of nearly equal bubbles, driven close to their resonance frequency. The amplitude and the frequency of these oscillations are measured and they are in good agreement with the theoretical predictions. However, the experiments reveal a phenomenon of hysteresis between the approach and the separation stages of the oscillations, which cannot be explained by the conservative model used to study the bubbles relative motion. A qualitative explanation of this hysteresis is based on the deformations of the bubbles from their assumed spherical shape, which are observed during the experiments.

This work was supported by the NASA Microgravity Program under the grant number NAG3-1620.

REFERENCES

Bjerknes, V. F. K. 1906 *Fields of Force*. Columbia University Press.

Blake, F. G. Jr 1949 Bjerknes forces in stationary sound fields. *J. Acoust. Soc. Am.* **21**, 551.

Crum, L. A. 1975 Bjerknes forces on bubbles in a stationary sound field. *J. Acoust. Soc. Am.* **57**, Part I, 1363–1370.

Doinikov, A. A. 1996 Mutual interaction between a bubble and a drop in a sound field. *J. Acoust. Soc. Am.* **99**, 3373–3379.

Eller, A. I. 1968 Force on a bubble in a standing acoustic wave. *J. Acoust. Soc. Am.* **43**, 170–171.

Kapustina, O. A. 1970 Degassing of liquids. In *Physical Principles of Ultrasonic Technology* (ed. L. D. Rozenberg). Vol. 1, Part IV, pp. 422–427. Plenum Press.

Kornfeld, M. & Suvorov, L. 1944 On the destructive action of cavitation. *J. Appl. Phys.* **15**, 495–506.

Oguz, H. N. & Prosperetti, A. 1990 A generalization of the impulse and virial theorems with an application to bubble oscillations. *J. Fluid Mech.* **218**, 143–162.

Pelekasis, N. A. 1991 A study on drop and bubble dynamics via a hybrid boundary element-finite element methodology. PhD Thesis, State University of New York at Buffalo.

Pelekasis, N. A. & Tsamopoulos, J. A. 1993*a* Bjerknes forces between two bubbles. Part 1. Response to a step change in pressure. *J. Fluid Mech.* **254**, 467–499.

Pelekasis, N. A. & Tsamopoulos, J. A. 1993*b* Bjerknes forces between two bubbles. Part 2. Response to an oscillatory pressure field. *J. Fluid Mech.* **254**, 500–527.

Prosperetti, A. 1977 Thermal effects and damping mechanisms in the forced radial oscillations of gas bubbles in liquids. *J. Acoust. Soc. Am.* **61**, 17–27.

Prosperetti, A. 1984*a* Bubble phenomena in sound fields: part one. *Ultrasonics* **22**, 69–77.

Prosperetti, A. 1984*b* Bubble phenomena in sound fields: part two. *Ultrasonics* **22**, 115–123.

Zabolotskaya, E. A. 1983 Interaction of gas bubbles in a sound field. *Sov. Phys. Acoust.* **30**(5), 365–368.